Sonic Landau Levels and Synthetic Gauge Fields in Mechanical Metamaterials

Hamed Abbaszadeh,[1] Anton Souslov,[1,2] Jayson Paulose,[1,4] Henning Schomerus,[3] and Vincenzo Vitelli[1,2,*]
[1]*Instituut-Lorentz, Universiteit Leiden, Leiden 2300 RA, The Netherlands*
[2]*The James Franck Institute and Department of Physics, The University of Chicago, Chicago, Illinois 60637, USA*
[3]*Department of Physics, Lancaster University, Lancaster LA1 4YB, United Kingdom*
[4]*Departments of Physics and Integrative Biology, University of California, Berkeley, California 94720, USA*
(Received 8 October 2016; published 9 November 2017)

Mechanical strain can lead to a synthetic gauge field that controls the dynamics of electrons in graphene sheets as well as light in photonic crystals. Here, we show how to engineer an analogous synthetic gauge field for lattice vibrations. Our approach relies on one of two strategies: shearing a honeycomb lattice of masses and springs or patterning its local material stiffness. As a result, vibrational spectra with discrete Landau levels are generated. Upon tuning the strength of the gauge field, we can control the density of states and transverse spatial confinement of sound in the metamaterial. We also show how this gauge field can be used to design waveguides in which sound propagates with robustness against disorder as a consequence of the change in topological polarization that occurs along a domain wall. By introducing dissipation, we can selectively enhance the domain-wall-bound topological sound mode, a feature that may potentially be exploited for the design of sound amplification by stimulated emission of radiation (SASER, the mechanical analogs of lasers).

DOI: 10.1103/PhysRevLett.119.195502

Electronic systems subject to a uniform magnetic field experience a wealth of fascinating phenomena such as topological states [1] in the integer quantum Hall effect [2] and anyons associated with the fractional quantum Hall effect [3]. Recently, it has been shown that in a strained graphene sheet, electrons experience external potentials that can mimic the effects of a magnetic field, which results in the formation of Landau levels and edge states [4,5]. Working in direct analogy with this electronic setting, pseudomagnetic fields have been engineered by arranging CO molecules on a gold surface [6] and in photonic honeycomb-lattice metamaterials [7,8].

In this Letter, we apply insights about wave propagation in the presence of a gauge field to acoustic phenomena in a nonuniform phononic crystal, using the appropriate mechanisms of strain-phonon coupling and frictional dissipation, in contrast to those present in electronic and photonic cases. The acoustic metamaterial context in which we implement gauge fields provides us with significant control [9–11] over frequency, wavelength, and attenuation scales unavailable in the analogous electronic realizations. For example, a metamaterial composed of stiff (e.g., metallic) components of micron-scale length may be suitable for control over ultrasound with gigahertz-scale frequencies, whereas cm-scale metamaterials may provide control over kHz-scale sound waves. We develop two strategies for realizing a uniform pseudomagnetic field in a metamaterial based on the honeycomb lattice, i.e., "mechanical graphene" [12]. In the first strategy, we apply stress at the boundary to obtain nonuniform strain in the bulk, which leads to a Landau-level spectrum, whereas in the second strategy, we exploit built-in, nonuniform patterning of the local metamaterial stiffness. This second strategy shows how the unique controllability of metamaterials can lead to novel designs inaccessible in the electronic context, and may be useful in scaling up these phenomena to long acoustic waveguides.

We explore acoustic phenomena associated with the Landau-level spectrum. For example, the acoustic analog of Shubnikov–de Haas oscillations [13] corresponds to a sharp peak in the phonon density of states at the Landau-level frequency. In addition, sound modes are confined within a length scale set by the analog of the magnetic length. Even stronger confinement of sound modes can be engineered at a domain wall associated with a change in the effective mass of the phononic excitations, which localizes phonon modes that are analogous to the topological domain-wall states in the Su-Schrieffer-Heeger model of polyacetylene [14]. We show how this domain-wall-bound mode exhibits robustness against a type of disorder that may come in the manufacturing of acoustic metamaterials—disorder in the stiffness of each component. Like other realizations of topological states [15,16] in mechanical [17–27], acoustic [28–36], and photonic [37] metamaterials, this characterization may help with the design of robust devices. We show that introducing dissipation on just one of the two sublattices enhances the domain-wall-bound sound mode. This feature may be implemented in the acoustic context using a material immersed in a viscous fluid (appropriate for low-Reynolds number, e.g., microscale metamaterials), or by including dampers (e.g., small dashpot dampers at every component for cm-scale realizations) within the material design. We suggest this feature may be exploited for the design of acoustic couplers, rectifiers, and sound amplification by stimulated emission of radiation (SASER).

Mechanical graphene.—We begin with a minimal, microscopic model of an acoustic metamaterial—a set of nodes positioned at the vertices of a honeycomb lattice and connected by rods to their nearest neighbors [see Fig. 1(a)] [12]. The compressional stiffness of the rods κ is determined by their fixed Young's modulus E, variable cross-section area S, and length a via ES/a. We assume the rods to be so slender that their bending stiffness is significantly lower than their compressional stiffness. We model the rods as central-force harmonic springs, whose elastic energy U is given in terms of the strain $\delta r/a$ by $U(\delta r) = \frac{1}{2}\kappa(|\mathbf{r}+\delta\mathbf{r}|-a)^2$. For small strains, this energy can be linearized in terms of node displacements $\mathbf{u}_1$ and $\mathbf{u}_2$ as $U(\mathbf{u}_1,\mathbf{u}_2) = \frac{1}{2}\kappa(\mathbf{e}\cdot[\mathbf{u}_1-\mathbf{u}_2])^2$, where $\mathbf{e}\equiv\mathbf{r}/|\mathbf{r}|$ is the unit vector along the spring. [In Fig. 1(a), we define the initial configuration for the node positions and stiffnesses.] Given this potential, we examine the linear equation of motion for acoustic vibrations of the lattice:

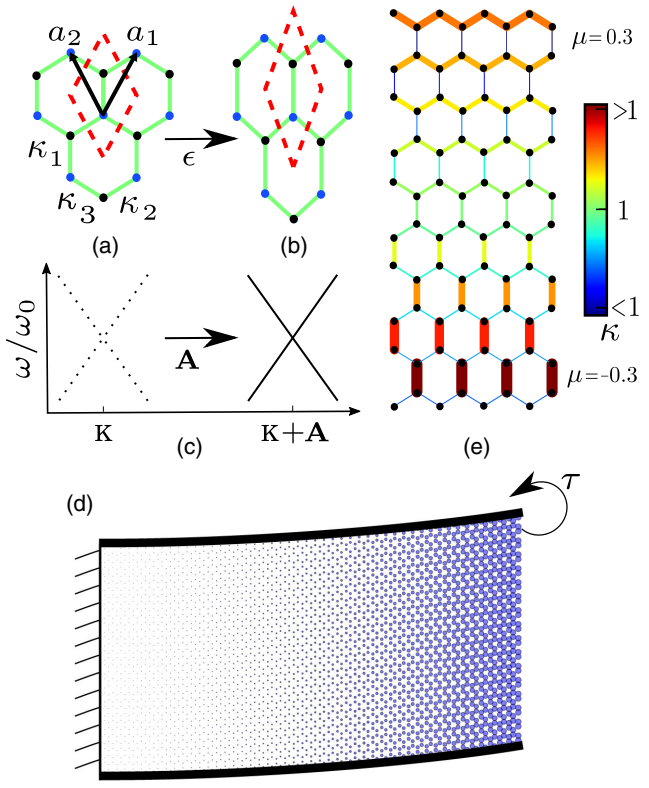

FIG. 1. (a) Mechanical graphene—a set of rods and nodes based on the honeycomb structure. The dashed line indicates the shape of a unit cell. (b) The lattice with a pure shear strain. (c) The shift of a Dirac point within the phonon spectrum of mechanical graphene due to the applied strain can be used to define an effective vector potential. (d) An externally applied nonuniform pure shear deformation that corresponds to a constant magnetic field. The external stress is applied by a torque τ on the boundary rods. (e) A nonuniform patterning of the local material stiffness that leads to a constant magnetic field. We consider periodic boundary conditions along x and free boundary conditions along y.

$$-m\ddot{u}_i^\alpha = \frac{\partial U}{\partial u_i^\alpha} = \sum_{j,\beta} D_{ij}^{\alpha\beta} u_j^\beta, \tag{1}$$

where u_i^α are the $\alpha = x, y$ components of displacement of the ith site and $D_{ij}^{\alpha\beta}$ are components of the dynamical matrix. In a periodic lattice, the solutions to this equation of motion are plane waves $\mathbf{u}_\mathbf{q} e^{i(\omega(\mathbf{q})t-\mathbf{q}\cdot\mathbf{x})}$, where both the dispersion relation $\omega(\mathbf{q})$ and the normal modes $\mathbf{u}_\mathbf{q}$ are found from the corresponding eigenvalue problem for each wave vector $\mathbf{q}$.

To lowest order in perturbation theory around point K [defined by $\mathbf{q}_K \equiv (0, 4\pi/3\sqrt{3}a)$], the dynamical matrix for the two bands near the frequency $\omega_0 \equiv \sqrt{3\kappa/2m}$ reduces to [38]

$$D = -\frac{1}{2}\omega_0^2(a\delta\mathbf{q}+\mathbf{A})\cdot\boldsymbol{\sigma} + (1+V)\omega_0^2\mathbb{I}, \tag{2}$$

where $\mathbb{I}$ is the 2×2 identity matrix, $\delta\mathbf{q}\equiv\mathbf{q}-\mathbf{q}_K$, and $\boldsymbol{\sigma}\equiv(\sigma_x,\sigma_y)$ contains Pauli spin matrices. The gauge field $\mathbf{A}$ and potential V are both zero for the homogeneous honeycomb lattice. From the structure of Eq. (2), we note that the dispersion around $\mathbf{q}_K$ has the form of a Dirac cone; i.e., two bands touch at the Dirac point [39].

Synthetic gauge field.—We now proceed to show that unlike uniform lattice deformations that merely shift this Dirac cone in wave vector space, nonuniform deformations can lead to an effective synthetic gauge field for sound. For uniform strain [Fig. 1(b)], $\mathbf{A}$ and V are both constant throughout the lattice. On the other hand, for a nonuniform but slowly varying strain, the position of the local Dirac point varies from one region to another [Fig. 1(c)], which corresponds to spatially dependent fields $\mathbf{A}$ and V. In terms of the affine component $\mathbf{U}$ and nonaffine component $\mathbf{W}$ of the displacement denoting, respectively, common and relative displacements of the two sublattices,

$$\mathbf{A}(x,y) = a(\mathbf{q}_K\cdot\nabla)\mathbf{U} + 3(\epsilon_{\rm ps}, -\epsilon_{xy}) + (W_y, -W_x)/a,$$

and $V = \frac{1}{2}\mathrm{Tr}\epsilon$, where $\epsilon_{ij}\equiv(\partial_i U_j + \partial_j U_i)/2$ is the linear affine strain and $\epsilon_{\rm ps}\equiv(\epsilon_{xx}-\epsilon_{yy})/2$ is its pure shear component.

To simplify the design of an acoustic device based on this strained lattice, we now consider those lattice strains that can be obtained by applying forces only on the boundary. Such a configuration requires that the forces in the bulk of the material balance each other. In the material we consider, this force-balance condition is satisfied provided that the nonaffine displacements depend on the affine strain via $W_x = \epsilon_{xy}a$ and $W_y = \epsilon_{\rm ps}a$. Thus, we obtain the following expression for the gauge field in a boundary-strained material:

$$\mathbf{A}(x,y;\epsilon) = a(\mathbf{q}_K\cdot\nabla)\mathbf{U} + 4(\epsilon_{\rm ps}, -\epsilon_{xy}). \tag{3}$$

For acoustic systems, we can also follow a second strategy: patterning the local material stiffness to achieve

a spatially dependent gauge field $\mathbf{A}$. For example, we can smoothly vary the composition or thickness of the rods to change their effective spring constants to $\kappa_i = \kappa + \delta\kappa_i$, where $i = 1, \ldots, 3$ labels springs in the lattice unit cell. We find that the gauge field and potential are given by

$$\mathbf{A}(x, y; \delta\kappa) = \left(-\frac{1}{3}\frac{2\delta\kappa_1 + \delta\kappa_2 + \delta\kappa_3}{\kappa}, \frac{\delta\kappa_2 - \delta\kappa_3}{\sqrt{3}\kappa} \right),$$
$$V = \frac{\delta\kappa_1 + \delta\kappa_2 + \delta\kappa_3}{3\kappa}. \quad (4)$$

To obtain a Landau-level spectrum, we select $\mathbf{A}$ and V such that (for units in which $a = 1$)

$$\nabla \times \mathbf{A} = B\hat{z} = \text{const}; \quad V = 0. \quad (5)$$

For any selection satisfying the conditions of Eqs. (5), the dynamical matrix in Eq. (2) has the form of the Hamiltonian for a Dirac electron in a plane with a constant magnetic field B applied perpendicular to that plane [41,42]. Let us now consider two practical solutions to Eqs. (5): (i) an externally applied nonuniform pure shear deformation, and (ii) nonuniform patterning of the spring constants along the y direction.

For case (i), we find the particle displacements throughout the lattice by substituting Eq. (3) into Eqs. (5) and solving the resulting partial differential equation: $\partial_y U_x + \partial_x U_y = -Bx/2$, with the additional constraint $\partial_x U_x = \partial_y U_y = 0$, which corresponds to nonvolumetric pure shear deformations. The resulting displacements satisfy $U_x = 0$ and $U_y = -Bx^2/4$. Note that for the honeycomb lattice, this condition can be realized using the boundary stresses illustrated in Fig. 1(d).

For case (ii), we substitute Eqs. (4) into Eqs. (5) to find the condition $\sqrt{3}\partial_x(\delta\kappa_2 - \delta\kappa_3) - \partial_y(\delta\kappa_2 + \delta\kappa_3) = 3\kappa B$ for the spatial dependence of the spring constants. We consider a material uniform along the x direction. This condition is satisfied for spring constants given by

$$\mu \equiv \frac{\delta\kappa_2}{\kappa} = \frac{\delta\kappa_3}{\kappa} = -\frac{\delta\kappa_1}{2\kappa} = \frac{By}{3}, \quad (6)$$

which is visualized in Fig. 1(e).

Mechanical Landau levels.—Now that we have proposed metamaterial architectures that realize the acoustic analog of a constant magnetic field, we go on to explore the physical consequences of this field for sound waves. To proceed, we focus on an architecture that is peculiar to the acoustic context; i.e., we select the realization of a patterned metamaterial waveguide described by Eqs. (6). Such a quasi-one-dimensional waveguide is uniform along the x axis, graded along the y axis, and is subject to no-stress boundary conditions on its top and bottom [see Fig. 1(e)]. The constant pseudomagnetic field leads to a Landau-level spectrum for frequencies near ω_0 [Fig. 2(a)].

Let us focus on the acoustic band corresponding to the most prominent Landau level: $n = 0$. In Fig. 2(b), this band is plotted for several values of the pseudomagnetic field B; as the pseudomagnetic field increases, the band flattens over a larger region in wave vector space, which leads to an increasing peak in the density of acoustic states [Fig. 2(d)]. The width of this flat region defines an inverse length scale ℓ^{-1}, which scales as $\ell^{-1} \sim \sqrt{B/a}$ [Fig. 2(c)]. This length scale is the acoustic analog of the magnetic length in a Landau level [39]. An acoustic mode in a Landau level has a Gaussian profile with a transverse confinement given by ℓ [Fig. 2(e)]. The transverse location of this mode within the waveguide is controlled by the mode wave number q_x, in contrast to an index-graded waveguide in which the location is determined by mode frequency. Consequently, in our case, the location of sound at a targeted frequency can be significantly tuned via the mode wave number (Fig. 2(e) and Ref. [39]).

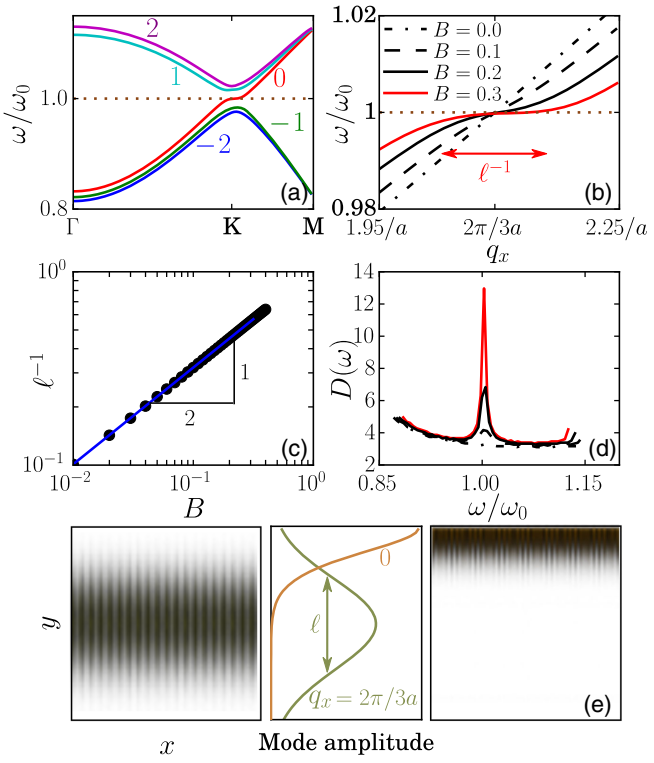

FIG. 2. Mechanical Landau levels: (a) A pseudomagnetic field leads to Landau levels around the Dirac point. (b) As the magnetic field increases, the zeroth-Landau-level band flattens. Band flatness can be characterized by the inverse magnetic length ℓ^{-1}. (c) The inverse magnetic length scales as the square root of the magnetic field. (d) Density of states for the zeroth Landau level, for the same values of B as in (b). The peak at the Dirac frequency rises as the bands flatten. (e) Visualizations of the zeroth Landau level at two different wave vectors. For $\mathbf{q} = \mathbf{q}_K$, this mode has a Gaussian profile around the waveguide center, whereas far from this point, at $\mathbf{q} = 0$, the mode decays exponentially away from the edge.

Sublattice-polarized domain wall modes.—The $n = 0$ Landau level at $q_x = q_{K,x} \equiv 2\pi/3a$ has frequency ω_K, is located at the waveguide center, and involves displacements exclusively on one sublattice. Modes with these properties generically appear in regions across which A_x

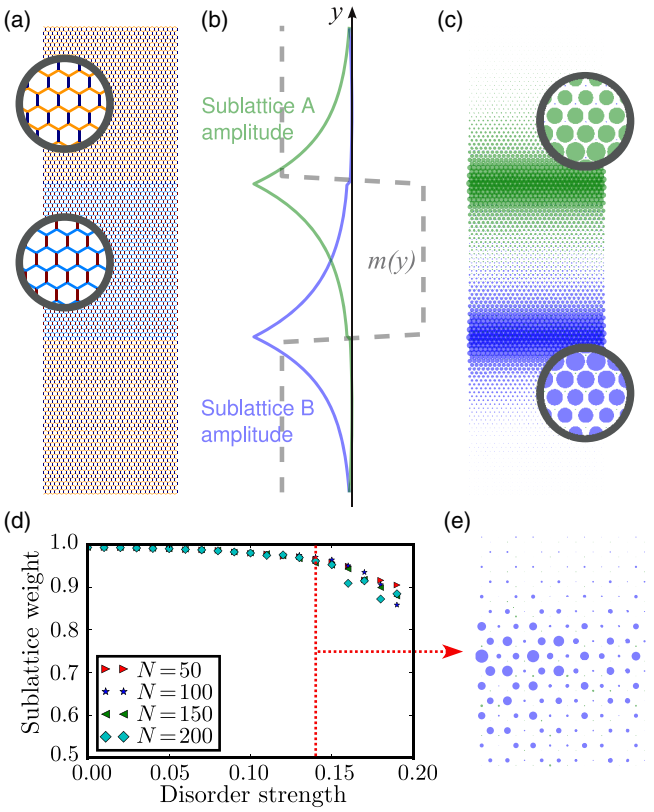

FIG. 3. (a) Waveguide with two domain walls separating two regions with $\mu = 0.08$ from a central region with $\mu = -0.08$. Bonds are colored according to their spring constants as in Fig. 1(e). Periodic boundary conditions are applied along x. (b) Variation of the effective Dirac mass $m(y)$ (dashed line) and midgap-mode amplitude for $q_x = 2\pi/3a$ on either sublattice (solid lines). (c) Visualization of midgap mode with sublattices distinguished, showing strong sublattice polarization. Each point on the A (B) sublattice is represented by a green (blue) disc whose area is proportional to the amplitude of the midgap mode. (d) Sublattice polarization of the domain-wall-bound mode in the presence of disorder in the spring constants [39]. (e) Even in the presence of strong (14%) disorder, we observe sublattice polarization due to the topological origin of the mode.

changes sign; i.e., their local dispersions have Dirac cones on opposite sides of point K. As an example, we consider a waveguide with two domain walls that separate a uniform central region with spring constants set by $\mu = -0.08$ from two regions, one above and one below, that each have $\mu = 0.08$ [Fig. 3(a)]. At $q_x = q_{K,x}$, the spectrum as a function of q_y near point K is described by a gapped 1D Dirac Hamiltonian centered about ω_K, with effective mass proportional to A_x [39]. The "spin" degree of freedom corresponds to the two sublattices of the honeycomb lattice: eigenstates of σ_z with eigenvalue ± 1 involve displacements solely on one sublattice. When the mass $m(y)$ varies spatially, domain walls at which $m(y)$ changes sign harbor exponentially localized midgap modes that are "spin-polarized," i.e., confined to a single sublattice [14,43].

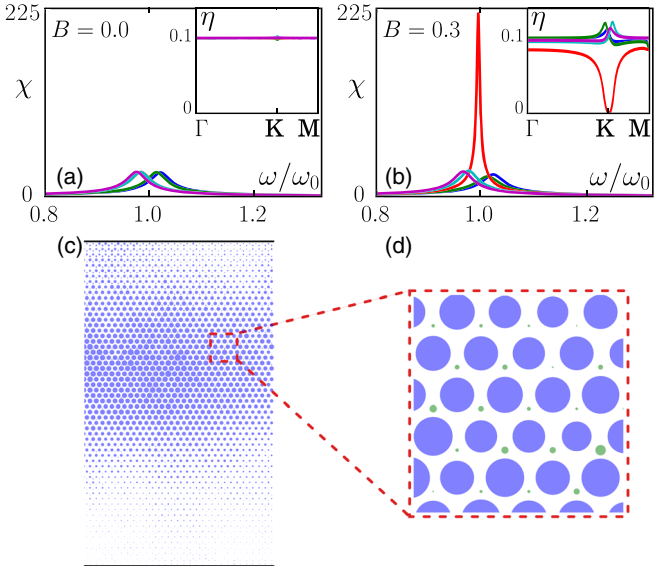

FIG. 4. Single-mode response χ of Landau-level states in mechanical graphene, including the effect of damping on one sublattice and for pseudomagnetic field values (a) $B = 0.0$ and (b) $B = 0.3$. Colors correspond to the different Landau-level bands identified in Fig. 2(a). Insets: Wave number dependent attenuation rate η of the corresponding bands. (c) The steady-state response (for $B = 0.3$) to external periodic forcing with frequency close to the Dirac frequency and at an edge that is situated 50 unit cells to the left of the section shown. Each point is represented by a disc whose area is proportional to the amplitude of the response. (d) Zoom-in of (c) shows that the Landau-level mode is selectively enhanced due to the presence of sublattice-biased damping.

The sublattice on which the mode is localized is determined by the sign of the change in mass upon crossing the domain wall. Figures 3(b) and 3(c) show the numerically obtained midgap mode for the domain wall geometry in Fig. 3(a), whose components on sublattice A (B) fall off exponentially from the top (bottom) domain wall. The robustness of the sublattice polarization under disorder in the spring constants is shown in Figs. 3(d) and 3(e) and is explained in the Supplemental Material [39].

Selective enhancement.—The sublattice polarization of the Landau-level states can be used to selectively enhance these modes under external drive by employing site-dependent damping. For example, for positive magnetic fields, the Landau-level states live only on the A sublattice of the honeycomb unit cell [4,41]. If we introduce damping of the form $-\gamma \dot{\mathbf{u}}_B$ into the equation of motion, Eq. (1), such that only the displacements of the B sublattice are damped, then the Landau-level acoustic waves would not be attenuated, whereas the rest of the sound waves, which generically are split between the A and B sublattices, would have a nonzero attenuation [39]. To characterize this selective enhancement, we study the attenuation rate $\eta(\mathbf{q})$ as a function of mode wave vector, as well as the self-response function $\chi(\omega)$ which measures the displacements in response to a drive at frequency ω [39]. In Figs. 4(a) and 4(b), we plot $\chi(\omega)$

and $\eta(\mathbf{q})$ for the Landau-level bands with $-2 \leq n \leq 2$, in response to an oscillatory drive that is proportional to the corresponding mode displacement vector. In the absence of the pseudomagnetic field B, the response is underdamped, but no mode stands out as having largest peak in χ [Fig. 4(a)], whereas for nonzero B, χ exhibits a strong peak at a frequency ω_0, corresponding to the zeroth Landau-level [Fig. 4(b)]. Therefore, when an edge of the metamaterial is driven near ω_0, the pseudomagnetic field combined with selective damping leads to selective enhancement of acoustic Landau-level modes [Figs. 4(c) and 4(d)] relative to the rest of the attenuated acoustic spectrum.

Towards mechanical lasers.—This phenomenon is the acoustic analog of selective enhancement of microwave modes realized in Ref. [44]. Just as selective enhancement for light waves may lead to the design of novel parity-time-symmetric [45,46] and topological [8] lasers, analogously, selective enhancement of sound waves may be useful in the design of sound amplification by stimulated emission of radiation (SASER), i.e., the acoustic analog of lasers, acoustic couplers, and rectifiers. The design of such devices [47] would involve acoustic resonators, acoustic drive, and nonlinearity of response. A potential architecture for this device may involve resonators at every node in the metamaterial, with an external acoustic source populating the states within each resonator.

We gratefully acknowledge funding from FOM, NWO, and Delta Institute for theoretical physics (H. A., A. S., J. P., and V. V.) and from EPSRC Programme Grant No. EP/N031776/1 (H. S.). This work was partially supported by the University of Chicago Materials Research Science and Engineering Center, which is funded by the National Science Foundation under Award No. DMR-1420709.

H. A. and A. S. contributed equally to this work.

Note added.—Recently, we learned about Ref. [48] that examines Landau levels in metamaterials composed of acoustic resonant cavities.

*vitelli@uchicago.edu

[1] C. L. Kane and E. J. Mele, Phys. Rev. Lett. **95**, 146802 (2005).
[2] M. Z. Hasan and C. L. Kane, Rev. Mod. Phys. **82**, 3045 (2010).
[3] R. B. Laughlin, Phys. Rev. Lett. **50**, 1395 (1983).
[4] F. Guinea, M. I. Katsnelson, and A. K. Geim, Nat. Phys. **6**, 30 (2010).
[5] N. Levy, S. A. Burke, K. L. Meaker, M. Panlasigui, A. Zettl, F. Guinea, A. H. Castro Neto, and M. F. Crommie, Science **329**, 544 (2010).
[6] K. K. Gomes, W. Mar, W. Ko, F. Guinea, and H. C. Manoharan, Nature (London) **483**, 306 (2012).
[7] M. C. Rechtsman, J. M. Zeuner, A. Tünnermann, S. Nolte, M. Segev, and A. Szameit, Nat. Photonics **7**, 153 (2013).
[8] H. Schomerus and N. Y. Halpern, Phys. Rev. Lett. **110**, 013903 (2013).
[9] L. Wu and L. Chen, J. Appl. Phys. **110**, 114507 (2011).
[10] F. Casadei, T. Delpero, A. Bergamini, P. Ermanni, and M. Ruzenne, J. Appl. Phys. **110**, 013903 (2012).
[11] K. H. Matlack, M. Serra-Garcia, A. Palermo, S. D. Huber, and C. Daraio, arXiv:1612.02362.
[12] T. Kariyado and Y. Hatsugai, Sci. Rep. **5**, 18107 (2016).
[13] L. Shubnikov and W. J. de Haas, Comm. Phys. Lab. Univ. Leiden **207a** (1930).
[14] W. P. Su, J. R. Schrieffer, and A. J. Heeger, Phys. Rev. Lett. **42**, 1698 (1979).
[15] E. Prodan and C. Prodan, Phys. Rev. Lett. **103**, 248101 (2009).
[16] N. Berg, K. Joel, M. Koolyk, and E. Prodan, Phys. Rev. E **83**, 021913 (2011).
[17] C. L. Kane and T. C. Lubensky, Nat. Phys. **10**, 39 (2013).
[18] H. C. Po, Y. Bahri, and A. Vishwanath, Phys. Rev. B **93**, 205158 (2016).
[19] B. G. Chen, N. Upadhyaya, and V. Vitelli, Proc. Natl. Acad. Sci. U.S.A. **111**, 13004 (2014).
[20] L. M. Nash, D. Kleckner, A. Read, V. Vitelli, A. M. Turner, and W. T. M. Irvine, Proc. Natl. Acad. Sci. U.S.A. **112**, 14495 (2015).
[21] J. Paulose, B. G. Chen, and V. Vitelli, Nat. Phys. **11**, 153 (2015).
[22] J. Paulose, A. S. Meeussen, and V. Vitelli, Proc. Natl. Acad. Sci. U.S.A. **112**, 7639 (2015).
[23] D. Z. Rocklin, B. G. Chen, M. Falk, V. Vitelli, and T. C. Lubensky, Phys. Rev. Lett. **116**, 135503 (2016).
[24] D Z. Rocklin, S. Zhou, K. Sun, and X. Mao, Nat. Commun. **8**, 14201 (2017).
[25] R. Süsstrunk and S. D. Huber, Science **349**, 47 (2015).
[26] B. G. Chen, B. Liu, A. A. Evans, J. Paulose, I. Cohen, V. Vitelli, and C. D. Santangelo, Phys. Rev. Lett. **116**, 135501 (2016).
[27] A. S. Meeussen, J. Paulose, and V. Vitelli, Phys. Rev. X **6**, 041029 (2016).
[28] A. B. Khanikaev, R. Fleury, S. H. Mousavi, and A. Alù, Nat. Commun. **6**, 8260 (2015).
[29] Z. Yang, F. Gao, X. Shi, X. Lin, Z. Gao, Y. Chong, and B. Zhang, Phys. Rev. Lett. **114**, 114301 (2015).
[30] P. A. Deymier, K. Runge, N. Swinteck, and K. Muralidharan, Comptes Rendus—Mecanique **343**, 700 (2015).
[31] S. H. Mousavi, A. B. Khanikaev, and Z. Wang, Nat. Commun. **6**, 8682 (2015).
[32] Y. T. Wang, P. G. Luan, and S. Zhang, New J. Phys. **17**, 073031 (2015).
[33] P. Wang, L. Lu, and K. Bertoldi, Phys. Rev. Lett. **115**, 104302 (2015).
[34] M. Xiao, W. J. Chen, W. Y. He, and C. T. Chan, Nat. Phys. **11**, 920 (2015).
[35] R. Süsstrunk and S. D. Huber, Proc. Natl. Acad. Sci. U.S.A. **113**, E4767 (2016).
[36] C. Brendel, V. Peano, O. Painter, and F. Marquardt, Proc. Natl. Acad. Sci. U.S.A. **114**, E3390 (2017).
[37] L. Lu, J. D. Joannopoulos, and M. Soljačić, Nat. Photonics **8**, 821 (2014).
[38] Near the point K' ($\mathbf{q}_{K'} = -\mathbf{q}_K$), the analogous expression differs only by $\mathbf{A} \to -\mathbf{A}$.

[39] See Supplemental Material at http://link.aps.org/supplemental/10.1103/PhysRevLett.119.195502 for further explanations, which includes Ref. [48].
[40] C. Herring, Phys. Rev. **52**, 365 (1937).
[41] R. Jackiw, Phys. Rev. D **29**, 2375 (1984).
[42] G. W. Semenoff, Phys. Rev. Lett. **53**, 2449 (1984).
[43] R. Jackiw and C. Rebbi, Phys. Rev. D **13**, 3398 (1976).
[44] C. Poli, M. Bellec, U. Kuhl, F. Mortessagne, and H. Schomerus, Nat. Commun. **6**, 6710 (2015).
[45] H. Hodaei, M. Miri, M. Heinrich, D. N. Christodoulides, and M. Khajavikhan, Science **346**, 975 (2014).
[46] Liang Feng, Zi Jing Wong, Ren-Min Ma, Yuan Wang, and Xiang Zhang, Science **346**, 972 (2014).
[47] I. Mahboob, K. Nishiguchi, A. Fujiwara, and H. Yamaguchi, Phys. Rev. Lett. **110**, 127202 (2013).
[48] Z. Yang, F. Gao, Y. Yang, and B. Zhang, Phys. Rev. Lett. **118**, 194301 (2017).